Atmos. Chem. Phys. Discuss., 13, 6923–6969, 2013
www.atmos-chem-phys-discuss.net/13/6923/2013/
doi:10.5194/acpd-13-6923-2013

Atmospheric Chemistry and Physics Discussions

A comparison of atmospheric composition using the Carbon Bond and Regional Atmospheric Chemistry Mechanisms

G. Sarwar[1], J. Godowitch[1], B. Henderson[2], K. Fahey[1], G. Pouliot[1], W. T. Hutzell[1], R. Mathur[1], D. Kang[3], W. S. Goliff[4], and W. R. Stockwell[5]

[1]Atmospheric Modeling and Analysis Division, National Exposure Research Laboratory, US Environmental Protection Agency, RTP, NC 27711, USA
[2]Environmental Engineering Sciences, University of Florida, Gainesville, FL 32611, USA
[3]Computer Sciences Corporation, RTP, NC 27709, USA
[4]College of Engineering Center for Environmental Research and Technology, University of California at Riverside, Riverside, CA 92507, USA
[5]Department of Chemistry, Howard University, Washington, DC 20059, USA

Received: 22 February 2013 – Accepted: 28 February 2013 – Published: 14 March 2013

Correspondence to: G. Sarwar (sarwar.golam@epa.gov)

Published by Copernicus Publications on behalf of the European Geosciences Union.

Abstract

We incorporate the recently developed Regional Atmospheric Chemistry Mechanism (version 2, RACM2) into the Community Multiscale Air Quality modeling system for comparison with the existing 2005 Carbon Bond mechanism with updated toluene chemistry (CB05TU). Compared to CB05TU, RACM2 enhances the domain-wide monthly mean hydroxyl radical concentrations by 46 % and nitric acid by 26 %. However, it reduces hydrogen peroxide by 2 %, peroxyacetic acid by 94 %, methyl hydrogen peroxide by 19 %, peroxyacetyl nitrate by 40 %, and organic nitrate by 41 %. RACM2 predictions generally agree better with the observed data than the CB05TU predictions. RACM2 enhances ozone for all ambient levels leading to higher bias at low (< 60 ppbv) concentrations but improved performance at high (>70 ppbv) concentrations. The RACM2 ozone predictions are also supported by increased ozone production efficiency that agrees better with observations. Compared to CB05TU, RACM2 enhances the domain-wide monthly mean sulfate by 10 %, nitrate by 6 %, ammonium by 10 %, anthropogenic secondary organic aerosols by 42 %, biogenic secondary organic aerosols by 5 %, and in-cloud secondary organic aerosols by 7 %. Increased inorganic and organic aerosols with RACM2 agree better with observed data. While RACM2 enhances ozone and secondary aerosols by relatively large margins, control strategies developed for ozone or fine particles using the two mechanisms do not differ appreciably.

1 Introduction

The composition of the atmosphere is understood through a combination of measurements and model predictions. Since measurements of composition are sparse in space, time, and chemical species; results of atmospheric chemical transport models fill in the gaps. Atmospheric chemical transport models are also used to develop air pollution control strategies to improve air quality for areas that do not meet ambient

standards. Chemical transport models have many components, each of which has associated uncertainty. The model framework includes transport algorithms, deposition processes, meteorological fields, emissions, and atmospheric chemistry. The model's atmospheric chemistry is represented by a gas-phase chemical mechanism. This study isolates the impact of atmospheric chemistry by implementing two different chemical mechanisms in a single chemical transport model.

Chemical mechanisms are continually updated to better represent laboratory studies and then tested in transport models. This summary will refer to three chemical mechanism series: State Air Pollution Research Center (SAPRC; e.g. Carter, 1990, 2000, 2010), Carbon Bond (CB; e.g. Gery et al., 1989), and the Regional Atmospheric Chemistry Mechanism (RACM; e.g. Stockwell, 1997). The SAPRC mechanism is not used in this study, but like CB and RACM has had several generations (Carter, 1990, 2000, 2010). The CB mechanism was originally developed in the 1980's, and the fourth version (CB-IV) is widely used in urban to regional chemical transport models. Yarwood et al. (2005) updated CB-IV, now CB05, to accurately simulate pristine, wintertime, and high altitude conditions. Recently, Whitten et al. (2010) updated CB's toluene chemistry in CB05TU. The RACM mechanism (Stockwell et al., 1997) was derived from the Regional Acid Deposition Model (Stockwell, 1986; Stockwell et al., 1990) specifically to address regional application. Goliff et al. (2013) recently updated the RACM mechanism to version 2 (RACM2).

The development of mechanisms is typically based on smog-chamber studies, and subsequent studies evaluate the impact on chemical transport model predictions. In CMAQ, several studies have examined the impacts of CB-IV, CB05, SAPRC99, and SAPRC07 (Sarwar et al., 2008, 2011; Luecken, et al., 2008; Faraji et al., 2008; Cai et al., 2011; Hutzell, et al., 2012; Shearer et al., 2012). Only two regional modeling studies, with a European model, have focused on RACM2. Kim et al. (2009, 2011) compared an early version of RACM2 to CB05 over Europe and found increases in ozone (by +5 %) and most aerosols (sulfate (SO_4^{2-}) by +16 %, nitrate (NO_3^-) by +11 %, ammonium (NH_4^+) by +10 %) except for secondary organic aerosols (SOA) (anthro-

pogenic SOA by −22 %, biogenic SOA by −1 %). The impact of RACM2 on model predictions over the US is unknown since both previous RACM2 studies were conducted over Europe. The US contains a large range of meteorological and emission conditions controlling the formation of secondary pollutants, and therefore it provides a good region to examine the impacts of new chemical mechanisms. Here, we describe the impacts of CB05TU and RACM2 on model predictions using a chemical transport model.

2 Methodology

2.1 Model framework

The Community Multiscale Air Quality (CMAQ) modeling system is a three-dimensional chemical transport model and incorporates major atmospheric processes (Byun and Schere, 2006). Prior studies suggest that CMAQ can reasonably simulate atmospheric pollutants (e.g. Eder and Yu, 2006; Appel et al., 2007; Foley et al., 2010). We use the current CMAQ model (version 5) for this study (http://www.cmascenter.org). The horizontal domain covers the continental United States discretized using a 12-km grid resolution while the vertical extent consists of 35 layers and extends up to 50 hPa. Results from a global model (GEOS-CHEM, Bey et al., 2001) are used to derive boundary conditions for the study. The model used clean air vertical profiles as initial conditions and a ten-day spin-up period. The Weather Research and Forecasting (version 3.3) model (Skamarock et al., 2008) using an updated four-dimensional data assimilation approach (Gilliam et al., 2012) generated the meteorological fields for the study. The Meteorology-Chemistry Interface Processor was applied to develop the meteorological input data sets for the subsequent CMAQ simulations since these model runs were exercised in an off-line mode. Gilliam and Pleim (2010) discussed performances for retrospective meteorological models. Meteorological fields used in the study are deemed

adequate since the bias and error are better than those indicated by Gilliam and Pleim (2010).

2.2 Gas-phase chemistry

2.2.1 CB05TU chemistry

Details of the CB05TU chemistry have previously been described elsewhere (Yarwood et al., 2005; Whitten et al., 2010); only a brief summary is provided here. CB05TU uses a lumped structure approach for representing atmospheric chemistry. It consists of 172 chemical reactions including 20 photolytic reactions and uses 65 chemical species to describe atmospheric chemistry (Table 1). It uses kinetic data from the National Aeronautics and Space Administration/Jet Propulsion Laboratory (NASA/JPL) (Sander et al., 2003) and the International Union of Pure and Applied Chemistry (IUPAC) (Atkinson et al., 2005) review panels. The mechanism evaluation was completed by performing chamber simulations and comparing the simulation results with experimental data from the University of California, Riverside and the University of North Carolina, Chapel Hill. It contains the bimolecular and ter-molecular hydrolysis of dinitrogen pentoxide (N_2O_5). However, following the recent International Union of Pure and Applied Chemistry (IUPAC, 2010) recommendation, in the modified version used here, we (1) removed the ter-molecular hydrolysis of N_2O_5 and (2) lowered the rate constant for the bimolecular hydrolysis of N_2O_5. CB05TU also accounts for the production of sulfuric acid via the reaction of hydroxyl radical (HO) and sulfur dioxide (SO_2). However, we updated the rate constant of the reaction following the recent NASA/JPL recommendation which is also consistent with the value used in RACM2.

2.2.2 RACM2 chemistry

The RACM2 mechanism described in Goliff et al. (2013) uses a lumped molecular approach for representing atmospheric chemistry. It consists of 363 chemical reactions

including 33 photolytic reactions among 120 chemical species (Table 2). It uses kinetic data from several sources including the recent suggestions of IUPAC (IUPAC, 2010) and NASA/JPL (Sander et al., 2011). The mechanism evaluation was completed by performing chamber simulations and comparing the simulation results with experimental data from the EXACT campaign and the University of California, Riverside. It contains only the bimolecular hydrolysis of N_2O_5. Similar to CB05TU, we used the rate constant for the bimolecular hydrolysis of N_2O_5 following the recent IUPAC recommendation. It also accounts for the gas-phase production of sulfuric acid via the reaction of HO and SO_2.

2.3 Emissions

The mapping of emissions of real organic species to emissions of mechanism species is a key component in the effective use of condensed mechanism in air pollution models. The assignments for the CB05TU and RACM2 mechanisms were developed and can be obtained at http://www.engr.ucr.edu/~carter/emitdb. The 2005 National Emissions Inventory (http://www.epa.gov/ttn/chief/net/2005inventory.html#inventorydata) was used as the starting point for generating model ready emissions. Emissions previously prepared for the AQMEII phase 1 project (Pouliot et al., 2012) were re-processed for CB05TU and RACM2. All other inputs needed for emission processing were unchanged for this study. The Sparse Matrix Operator Kernel Emissions (SMOKE) system (Houyoux et al., 2000) was used to generate hourly, gridded, and speciated model ready emissions. All of the ancillary SMOKE inputs were based on the Version 4.2 2005 Modeling Platform (http://www.epa.gov/ttn/chief/emch/index.html#2005). Biogenic emissions were prepared using the Biogenic Emissions Inventory System (version 3.14) (Schwede et al., 2005).

2.4 Aerosol chemistry

The details of the CMAQ aerosol chemistry have been described in other studies (Binkowski and Roselle, 2003; Byun and Schere, 2006; Carlton et al., 2010). CMAQ describes the aerosol size distribution using three lognormal modes (Aitken, accumulation, and coarse). Aerosol species considered in CMAQ include inorganic aerosols, organic aerosols, sodium chloride, crustal materials, and other unspeciated material (Appel et al., 2013). Aqueous-phase oxidation of S(IV) by hydrogen peroxide (H_2O_2), O_3, oxygen catalyzed by manganese (Mn^{2+}) and iron (Fe^{3+}), methylhydroperoxide (MEPX), and peroxyacetic acid (PACD) produce sulfate. Sarwar et al. (2013) describes the details of the chemical reactions in aqueous-phase. The model also accounts for the production of nitric acid (HNO_3) via the heterogeneous hydrolysis of N_2O_5. It currently uses the Davis et al. (2008) parameterization for the heterogeneous uptake coefficient that accounts for impacts of particle composition, water, phase of the particulate matter and temperature. CMAQv5.0 uses ISORROPIA II (Fountoukis and Nenes, 2007) to determine partitioning of inorganics between gas and aerosol phases.

The SOA in CMAQ is comprised of the contributions from anthropogenic sources, biogenic sources, and in-cloud processes. A detailed description of the SOA in CMAQ has been provided elsewhere (Carlton et al., 2010). Anthropogenic SOA is formed from the reactions of benzene, toluene, and xylene that produce organic peroxy radicals. These peroxy radicals react with nitric oxide (NO) to produce semi-volatile organic compounds or react with hydrogen peroxy radical (HO_2) to produce non-volatile SOA. Biogenic SOA is formed from the reactions of isoprene, monoterpene, and sesquiterpene that produce semi-volatile organic compounds. The model also accounts for acid enhanced pathway for isoprene SOA formation. Semi-volatile organics from anthropogenic and biogenic sources partition and form SOA. Semi-volatile organics also form non-volatile oligomers through particle phase-reactions. In-cloud SOA is formed from the aqueous-phase oxidation of glyoxal and methylglyoxal (Carlton et al., 2008, 2010). Glyoxal is not explicitly represented in CB05TU; therefore methylglyoxal with a Henry's

Law coefficient adjusted to that of glyoxal is used to represent in-cloud SOA production when using CB05TU (Carlton et al., 2010). In contrast, RACM2 contains both glyoxal and methylglyoxal and are used explicitly in the model to produce in-cloud SOA.

2.5 Simulation details

Two simulations, one with each chemical mechanism, were completed for the month of September 2006. The US O_3 season, a period marked by elevated regional O_3 concentrations, runs from May through September. The 2006 Texas Air Quality Study (TexAQS) was conducted during August–September (Parrish et al., 2009) and thus the simulation period allows for a comparison of model predictions with observations from the 2006 TexAQS. The first simulation used CB05TU while the second simulation used RACM2. Differences in the results between the two simulations can thus be attributed to the differences in the chemical mechanisms. A third order numerical solver based on the Rosenbrock method (Sandu et al., 1997) was used to solve the system of ordinary differential equations representating gas-phase chemistry. The use of RACM2 increases computational time of the model by 37 % compared to that of CB05TU. It should be noted that the increase is due to the combination of an increased number of chemical species in the chemistry as well as an increase in the number of transported species.

3 Results and discussions

3.1 Impact on key oxidants

3.1.1 Impact on hydroxyl radical (HO)

The importance of atmospheric HO is well established since it reacts with most atmospheric compounds and determines atmospheric oxidation capacity. The CB05TU predicted domain-wide monthly averaged HO is 0.05 pptv while the RACM2 predicted

value is 0.07 pptv; thus, RACM2 enhances overall HO by 46 % (Table 3). Spatially resolved monthly mean HO obtained with CB05TU and the percent differences between RACM2 and CB05TU are shown in Fig. 1a, b. Spatially, the predicted mean HO with CB05TU ranged between 0.02–0.12 pptv with southern areas showing higher concentrations than northern areas. The southern plain states and portions of California, for example, have the highest predicted concentrations. RACM2 enhances HO by 12–36 % in the eastern US and 36–60 % in the western US due to several factors. First, it produces more O_3 (described later) than CB05TU and thus generates more singlet oxygen atoms (O^1D) via photolysis that subsequently enhances the production of HO via a reaction with water vapor (H_2O). RACM2 also produces more HO than CB05TU from reactions of olefins and O_3 due to higher production yields. RACM2 contains additional reaction products that can subsequently produce HO. For example, methyl acrolein is not an explicit chemical species in CB05TU, but in RACM2 it is separate and directly produces HO from photolysis. RACM2 uses a rate constant suggested by Mollner et al. (2010) for the NO_2 + HO reaction which is lower than the value used in CB05TU. It reduces the loss of daytime HO and also enhances the concentration of HO in RACM2.

The few measurements of HO support RACM2's enhancement of HO. Measurements of atmospheric HO concentrations in Houston during the 2006 TexAQS have been reported by Mao et al. (2010a). Median predicted HO concentrations obtained with the two mechanisms are compared to the measurements in Houston in Fig. 1c. Both mechanisms capture the diurnal variation of the observed data; however, they both under-predict observed values both during the night and day. While CB05TU under-predicts the observed peak value by 30 %, RACM2 under-predicts observed HO by only 15 %. RACM2 captures the daytime observed values better than CB05TU.

3.1.2 Impact on hydrogen peroxide (H_2O_2)

H_2O_2 is the most efficient aqueous-phase oxidant for the conversion of S(IV) into S(VI) (Seigneur and Saxena, 1988). Spatial predictions of monthly mean H_2O_2 obtained

with CB05TU and the percent differences between the two mechanisms are shown in Fig. 2a, b. CB05TU predicts higher H_2O_2 values (> 0.8 ppbv) over the southern and western areas of the modeling domain. It predicts lower H_2O_2 values (< 0.6 ppbv) over Canada, the Midwest and Northeastern US. RACM2 decreases H_2O_2 by 9–15 % in most areas except in the Southwestern US where it decreases H_2O_2 by 3–9 %. In both mechanisms, H_2O_2 is produced from the reactions of $HO_2 + HO_2 = H_2O_2 + O_2$ and $HO_2 + HO_2 + H_2O = H_2O_2 + O_2 + H_2O$ while it is consumed by photolysis and the reaction with HO. The rate constant for the reaction of H_2O_2 and HO, and the photolysis rates are similar in both mechanisms. Unlike CB05TU, RACM2 produces H_2O_2 from alkene/O_3 reactions. However, their contributions are generally small and do not affect the overall production of H_2O_2. The rate constants for the reactions producing H_2O_2 are similar in both mechanisms. However, RACM2 produces lower H_2O_2 because it also predicts lower HO_2 except over salt-water bodies. Consistent with the enhanced HO_2 predictions over salt-water bodies, RACM2 increases H_2O_2 by 3–15 % over salt-water bodies.

Measurements of H_2O_2 for the simulation period are not readily available for comparison with model predictions. Sarwar et al. (2007) previously compared CB-IV and CB05 predicted H_2O_2 to observations from the 2001 Northeast Oxidant and Particle Study (NEOPS). Mean observed H_2O_2 was 0.80 ppbv compared to the CB05 prediction of 1.0 ppbv. The CB05TU predicted mean value for this study is 0.4 ppbv (the same location) while the RACM2 predicted mean value is 0.36 ppbv. Thus, the CB05 predicted value in 2001 is 2.5 times greater than the 2006 CB05TU predicted value. Assuming a proportional response in RACM2, we derive a RACM2 prediction of 0.91 ppbv for 2001. Thus, the RACM2 derived H_2O_2 prediction of 0.91 ppbv agrees better with the observed data of 0.80 ppbv than the CB05 prediction of 1.0 ppbv.

3.1.3 Impact on peroxyacetic acid (PACD)

PACD is an aqueous-phase oxidant that plays an important role in the conversion of S(IV) into S(VI). The spatial pattern of predicted PACD with CB05TU is similar to

that of H_2O_2 (Fig. 2c). CB05TU predicts higher values (> 0.4 ppbv) over the southern and western areas of the modeling domain. It predicts lower values (< 0.3 ppbv) over Canada, the Midwest and Northeastern US. RACM2 reduces PACD in most areas by 60–100 % (Fig. 2d). PACD is formed from the reactions of acetyl peroxy and higher acyl peroxy radicals with HO_2. In RACM2, yields of PACD productions from these reactions are only 50 % of those in CB05TU and predictions of HO_2, acetyl peroxy radical, higher peroxy radical are also lower than those obtained with CB05TU. Additionally RACM2 photolysis rates of PACD are about two times greater and the rate constant for the reaction of PACD with HO are also greater (7 times greater at 298 K and 1.0 atm) than those in CB05TU. Thus, RACM2 predicts much lower PACD concentrations compared to those with CB05TU.

Measurements of PACD for the simulation period are not readily available for comparison with model predictions. Zhang et al. (2010) measured PACD in an urban (Beijing) and two rural areas (Backgarden and Mazhuang) in China. Measurements were conducted at three different periods (2006, 2007, and 2008) in Beijing and one time period in Backgarden (2006) and Mazhuang (2008). We calculated mean values for the entire sampling period from reported daytime and nighttime mean values. The mean value for Beijing is 34 pptv in 2006, 113 pptv in 2007, and 36 pptv in 2008. The mean value for Backgarden is 27 pptv and for Mazhuang is 117 pptv. CB05TU predicted monthly mean in southern and western areas of the modeling domain range between 500–1000 pptv while predictions for the northern area range between 50–300 pptv. RACM2 predicted monthly mean in the southern and western areas range between 30–60 pptv while predictions for the northern area generally range between 10–30 pptv. We also analyzed CB05TU predictions for a summer month (July) in 2006. Predicted values are even greater than the predictions in September. Assuming similar order of magnitude ambient levels of PACD over China and over the US, the CB05TU predictions are too high while the RACM2 predictions appear to be about the right order of magnitude.

3.1.4 Impact on methylhydroperoxide (MEPX)

MEPX is also an oxidant for the aqueous-phase oxidation of S(IV) to S(VI). Similar to H_2O_2 and PACD, CB05TU predicts the higher MEPX levels (> 0.4 ppbv) over the southern and western areas of the modeling domain (Fig. 2e) and lower values (< 0.3 ppbv) in Canada, Midwest, and Northeastern US. RACM2 reduces MEPX over most land areas of the modeling domain by 24–40 % while increasing predicted values by 8–24 % over some water bodies (Fig. 2f). MEPX is formed from the reaction of methyl peroxy radical and HO_2 while it is consumed by photolysis and the reaction with HO. The rate constant for the reaction of MEPX and HO in RACM2 is lower (almost 30 % lower at 298 K and 1.0 atm) than that in CB05TU. RACM2 photolysis rates of MEPX are approximately 10 % greater than those in CB05TU which consumes more MEPX. The rate constant for the formation reaction is similar in both mechanisms. RACM2 predicts lower HO_2, thus the production rate of MEPX is also lower.

Measurements of MEPX for the simulation period are not readily available for comparison with model predictions. Sarwar et al. (2007) compared CB-IV and CB05 predicted MEPX to observations from the 2001 NEOPS. Mean observed MEPX was 0.30 ppbv compared to the CB05 prediction of 0.40 ppbv. The CB05TU predicted mean value for this study is 0.20 ppbv (at the same location) while the RACM2 predicted value is 0.15 ppbv. Thus, the CB05 prediction in 2001 was 1.96 times greater than the 2006 CB05TU prediction. Assuming a proportional response in RACM2, we derive a RACM2 predicted value of 0.29 ppbv for 2001. Thus, the RACM2 derived MEPX prediction of 0.29 ppbv agrees better with the observed data of 0.30 ppbv than the CB05 predicted value of 0.40 ppbv.

3.2 Impact on nitrogen species

3.2.1 Impact on total nitrate (TNO_3)

Predicted monthly mean TNO_3 with CB05TU and the percent differences between the two mechanisms are shown in Fig. 3a, b. Here TNO_3 represents the sum of HNO_3, fine-particulate nitrate, and coarse-particulate nitrate. CB05TU predicts the highest TNO_3 in southern California and the lowest TNO_3 in large areas of western US and Canada (Fig. 3a). CB05TU predicts concentrations of 0.5–1.5 ppbv over most of the eastern US. RACM2 increases TNO_3 by 30–50 % in some areas of southeastern US, coastal areas of the Gulf of Mexico, and some areas of the eastern seaboard, and 10–30 % in most of the eastern US and California. The important HNO_3 production pathways are the daytime production via the reaction of NO_2 and HO and the nighttime production via the homogeneous and heterogeneous hydrolysis of N_2O_5. The RACM2 rate constant for the reaction of NO_2 and HO is slightly lower than that of the CB05TU value. However, RACM2 predicted HO concentrations are greater than those obtained with CB05TU; consequently, the daytime production of HNO_3 by RACM2 is greater than that by CB05TU. In addition, a fraction of the reaction of NO and HO_2 in RACM2 produces HNO_3 which also contributes to the additional daytime HNO_3 production compared to that obtained with CB05TU. Changes in the nighttime production of HNO_3 between the two mechanisms are much smaller than that of the daytime production.

Predicted HNO_3 results are compared to measurements from the NOAA-WP3 research aircraft during the 2006 TexAQS (13 September) in Fig. 3c. Both mechanisms track the variation of observed concentrations outside and within the Dallas-Fort Worth urban plumes along the flight path. While CB05TU predictions generally follow the observed data, RACM2 predictions tend to slightly over-predict compared to the observed data. However, CB05TU under-predicts the first and the last observed peaks when RACM2 captures the observed data better. The overall slope of the fitted line of model predictions versus observations from multiple flights was 0.87 for CB05TU and 1.13 for RACM2. Similar results are obtained for comparisons with aircraft measurements

on other days as well as surface measurements from the Clean Air Status and Trends Network (CASTNET). We also compared CB05TU predictions from other model simulations to CASTNET measurements (not shown here) and found that it under-predicts HNO_3 compared to the observed data in summer months. Though RACM2 tended to overpredict HNO_3 in September, it may improve the model underpredictions in summer months.

3.2.2 Impact on peroxyacetyl nitrate (PAN)

Predicted monthly mean PAN with CB05TU and the percent differences between the two mechanisms are shown in Fig. 3d, e. CB05TU predicted monthly mean PAN concentrations are greater than 0.1 ppbv across the US. Concentrations greater than 0.4 ppbv are predicted in the Mid Atlantic States, Midwest, Southern Plains, California, and Idaho. The highest PAN is predicted in California while the lowest values are predicted in northern Canada. RACM2 decreases PAN by 36–60 % in Plain States, Midwest and California and 12–36 % in other areas. PAN is formed from the reaction of acetyl peroxy and nitrogen dioxide (NO_2). The primary reasons for the decrease in PAN with RACM2 are: (1) a lower rate constant (15 % lower at 298 K and 1.0 atm) for the PAN formation reaction (2) a higher rate constant for the thermal decomposition reaction of PAN, and (3) RACM2 contains two photolysis channels one of which produces acetyl peroxy, which can produce more PAN, while the other does not. CB05TU contains only one photolysis channel which produces acetyl peroxy that can recombine with NO_2 to reproduce PAN. RACM2 predicted acetyl peroxy radical is lower than that obtained with CB05TU which also contributes to the lower production of PAN. In addition, RACM2 also contains a reaction involving PAN and HO which consumes additional PAN though its impact is small. The increases in PAN with RACM2 in Idaho are primarily due to differences in speciation of biomass emissions and subsequent reactions.

Predicted PAN concentrations are compared to the aircraft measurements along the same flight path in Fig. 3f. Both mechanisms track the variation of observed PAN con-

centrations outside and within the Dallas-Fort Worth urban plumes along the flight path. However, CB05TU considerably over-predicts PAN compared to observed data, while RACM2 slightly under-predicts the observed data. Overall, CB05TU over-predicts PAN by 50 % compared to observed data, while RACM2 predictions are lower than observed values by 10 %. Predictions on other days also show similar agreement with observed data. Previous studies (Yu et al., 2010, 2012) comparing model predictions obtained with CBIV and CB05 mechanisms to observed PAN from several field campaigns have also noted that these mechanisms over-predict PAN. Thus, the chemistry in RACM2 has improved the predictions of PAN. Although not shown here, RACM2 also reduces the predictions of peroxypropionyl nitrate compared to those obtained with CB05TU by similar magnitudes.

3.2.3 Impact on organic nitrate (NTR)

CB05TU contains only one organic nitrate species (NTR) while RACM2 contains several organic nitrate species. All organic nitrate species in RACM2 are added for comparison with NTR of CB05TU. Predicted monthly mean NTR with CB05TU and the percent differences between the two mechanisms are shown in Fig. 3g, h. Predicted NTR concentrations with CB05TU are greater than 0.2 ppbv across the entire US. Values greater than 0.8 ppbv are predicted in the Southeastern US and California. RACM2 decreases NTR by 45–75 % in the Southwestern US and Mexico and 15–45 % in other areas due to several factors including: (1) NTR yields for many reactions in RACM2 are lower than those in CB05TU (2) the rate constant for the NTR + HO in RACM2 is 13 times greater than that in CB05TU and so consumes more NTR. As mentioned earlier, RACM2 produces greater HO than CB05TU; thus, the consumption of NTR via HO in RACM2 is substantially greater than in CB05TU. RACM2 increases NTR in Idaho primarily due to differences in speciation of biomass emissions and subsequent reactions. Measurements of organic nitrates are not readily available for the simulation period for comparison with model predictions.

3.2.4 Impact on secondary nitrogen species (NO_z)

Predicted monthly mean NO_z with CB05TU and the percent differences between the two mechanisms are shown in Fig. 4a, b. Here we define NO_z as the sum of all products of NO_x oxidation (i.e. secondary nitrogen species including gaseous and particulate nitrogen species; Trainer et al., 2000). Thus, NO_z for CB05TU is defined as $NO_z = NO_3 + 2 \times N_2O_5 + HONO + HNO_3 + PAN + PANX + PNA + NTR + CRON + CRNO + CRN2 + CRPX + OPAN + ANO_3$; where all gaseous chemical species are defined in Table 1 and ANO_3 is aerosol particulate nitrate. Similarly, NO_z for RACM2 is defined as $NO_Z = NO_3 + 2 \times N_2O_5 + HONO + HNO_3 + PAN + PPN + MPAN + HNO_4 + ISON + ONIT + NALD + ADCN + OLNN + OLND + ANO_3$; where all gaseous chemical species are defined in Table 2. CB05TU predicted NO_z concentrations are greater than 0.5 ppbv for all areas in the US. Values greater than 3.5 ppbv are predicted in southern California while 2.0–4.0 ppbv are predicted in the vicinity of major urban areas of the eastern US. RACM2 decreases NO_z by 24–40 % in areas of the Southwestern US, the Gulf of Mexico, and the Atlantic Ocean, and by 8–24 % in other areas. As discussed earlier, RACM2 enhances TNO_3 while decreasing predictions of PAN, PPN, and NTR compared to CB05TU. The decreases in PAN, PPN, and NTR overwhelm the increases in TNO_3; consequently, RACM2 decreases NO_z.

The major components of NO_z are TNO_3, PAN and NTR which account for 81 % in CB05TU (mean domain-wide value) and 84 % in RACM2. TNO_3 is the most dominant chemical species in mean NO_z accounting for 34 % of NO_z in CB05TU. NTR is the second most dominant chemical species and accounts for 29 % of NO_z in CB05TU. RACM2 lowers NTR by 41 % compared to that of CB05TU and is the primary reason for the reduction in NO_z. PAN accounts for 18 % of the mean NO_z in CB05TU. RACM2 lowers PAN by 40 % compared to CB05TU, which also contributes to the reduction in NO_z.

Both NO_y and NO_x concentrations are measured in the Southeastern Aerosol Research and Characterization (SEARCH) network. NO_z concentrations are derived by

subtracting NO_x from NO_y measurements and are compared to the predicted NO_z values for the Yorkville site in Fig. 4c. CB05TU over-predicts NO_z compared to the observed data while RACM2 predictions agree better with the observed data.

3.3 Impact on O_3

3.3.1 Impact on surface O_3

Predicted monthly mean O_3 with CB05TU and the percent differences between the two mechanisms are shown in Fig. 5a, b. Mean predicted O_3 concentrations are greater than 24 ppbv in all areas of the US. Predicted O_3 concentrations are the highest in southern California and the lowest in northern Canada. Predicted mean O_3 is lower in the eastern US than in the western US. Mean values are greater in the southern US and Mexico than those in the northern US and Canada. RACM2 increases O_3 in most of the modeling domain (Fig. 5b). The increases are greater (generally 6–12 %) in the southern area of the domain while smaller (0–6 %) increases are predicted in the northern area of the domain. Kim et al. (2009) also compared O_3 predictions from the two mechanisms over Europe and noted that RACM2 predicted higher O_3 than CB05. Several factors in RACM2 increase O_3 compared to CB05TU: (1) while the NO_2 photolysis rate in RACM2 is higher, the rate constant for the titration of O_3 by NO in RACM2 is lower (2) a lower rate constant for the $NO_2 + OH$ reaction, (3) NO_x recycling from organic nitrate and other species is greater in RACM2, and (4) some of the organic chemistry (especially aromatic chemistry) produces more RO_2 in RACM2; thus, the conversion of NO into NO_2 via the NO and RO_2 reaction is greater in RACM2. Kim et al. (2009) provides a more detailed description of the differences in the two mechanisms that lead to enhanced O_3 formation in RACM2.

Daily maximum 8-h O_3 concentrations are calculated using ambient monitoring data from the Air Quality System (AQS). Figure 5c presents the median and inter-quartile ranges of predicted values from both mechanisms compared to observed concentrations binned at 10 ppbv intervals. CB05TU over-predicts O_3 when observed concentrations are lower than 60 ppbv. RACM2 increases the O_3 bias over this lower concentration range. Both mechanisms perform relatively well at observed concentrations from 50–70 ppbv. Over 70 ppbv, CB05TU under-predicts while RACM2 improves the comparison. Thus, RACM2 better reproduces observed data at higher concentrations but over-predicts at lower concentrations.

3.3.2 Impact on diurnal and day-to-day variation of surface O_3

Hourly diurnal observed O_3 at AQS sites and the model predictions obtained with the two mechanisms are presented in Fig. 6. Predictions with both mechanisms track the diurnal pattern of observed O_3. However, nighttime predicted values obtained with CB05TU are 6–8 ppbv greater than the observed values. Nighttime O_3 over-predictions by atmospheric chemical transport models arise from model resolution artifacts and have been reported by other investigators (e.g. Arnold et al., 2006; Mao et al., 2010b). CB05TU predicted peak value exceeds the observed value by ~ 8 ppbv. RACM2 predicted values are greater than those with CB05TU and exceed the observed values by a slightly larger margin. Thus, RACM2 increases O_3 predictions at all hours compared to those obtained with CB05TU.

The time series of predicted daily maximum 8-h O_3 obtained with the two mechanisms are compared to the observed data at AQS sites in selected major urban areas (New York City, Atlanta, Houston, and Los Angeles) and are shown in Fig. 7a–d. Both models capture the day-to-day variation in observed data reasonably well. While CB05TU generally tracks observed O_3, it under-predicts O_3 when observed concentrations are high. For example, it under-predicts O_3 on 17 and 19 September in Los Angeles, 1, 7, 14, 20, 26, and 27 September in Houston, 22 and 28 September in Atlanta, 9, 22, and 27 September in New York while RACM2 improves predictions compared to the observed data on these days. Thus, increased O_3 with RACM2 produces mixed results; it deteriorates the comparison at low observed O_3 while improving the comparison at high observed O_3.

3.3.3 Impact on vertical distribution of O_3

Vertical profiles of O_3 obtained with CB05TU and RACM2 at 18:00 UTC on 13 September are presented in Fig. 8a. Data shown in the figure are obtained by averaging the domain-wide O_3. These vertical profiles reveal that RACM2 enhances O_3 not only at the surface but also aloft. It enhances O_3 up to about 14 000-m. Predictions on other days are also similar. Model predictions are compared to the aircraft measurements from the 2006 TexAQS in Fig. 8b (15 September). Differences in O_3 concentrations between the chemical mechanisms are also evident in a comparison to concentrations near 500 m above ground along the entire 5-h flight pattern of the NOAA WP-3 research aircraft, which consisted of horizontal traverses both upwind (over the Gulf of Mexico) and downwind crossings of the Houston, TX urban plume. RACM2 predicted O_3 concentrations are generally up to 5 ppbv higher than the CB05TU results. In addition, O_3 concentrations predicted by both mechanisms are overestimated in this case primarily due to the particularly high modeled background concentrations ($\sim$ 70 ppbv) relative to the observed values ($\approx$ 25–30 ppb) exhibited upwind of Houston over the Gulf area from hour 17:00 to 19:00 UTC. Excess O_3 (i.e. peak – background values) in the 4 urban plume crossings occurring between hour 19:00–21:00 UTC in the modeled results ($\approx$ 30 ppb) was less than that found in the observations ($\approx$ 40 ppb or more). Ozone formation by the chemical mechanisms is limited by the considerably underestimated modeled VOC emissions, as depicted in Fig. 8b with ethene concentrations. Observations were found to be considerably higher than modeled ethene concentrations, particularly in the peak concentrations observed within the urban plume which were as much as a factor of 5–10 greater than modeled values.

3.4 Impact on ozone production efficiency (OPE)

OPE has been defined by several investigators (e.g. Kleinman et al., 2002) and can be calculated from the slope from a linear regression of the relationship between daytime O_3 and NO_z concentrations and for aged air masses ($O_3/NO_x > 46$) (Arnold et al.,

2003). OPE calculated at three different sites using model predictions and measurements from the SEARCH network are presented in Fig. 9. For the Yorkville site, OPE derived from the measurements is 8.9. The CB05TU based value is only 5.4 while the RACM2-based value is 8.4. Thus, CB05TU under-predicts OPE while the RACM2 based value agrees better with the observation based value. A comparison of OPE derived from the Centerville and Oak Grove site measurements to model based values also shows similar results (Fig. 9b, c). RACM2 produces more O_3 while decreasing NO_z; hence it enhances OPE compared to that of CB05TU.

3.5 Impact on secondary aerosols

3.5.1 Impact on secondary inorganic aerosols

Predicted monthly mean SO_4^{2-} with CB05TU and the percent differences between the two mechanisms are shown in Fig. 10a, b. CB05TU predicts high SO_4^{2-} concentrations over the eastern-half of the US while predicting low concentrations in the western US. RACM2 increases SO_4^{2-} across the entire US compared to CB05TU. It increases SO_4^{2-} by 15–25 % in southern California, in a portion of Southern Plains, and by 5–15 % in other areas. While RACM2 enhances the production of SO_4^{2-} via the gas-phase SO_2 oxidation by HO and the aqueous-phase S(IV) oxidation by O_3, it decreases the production of SO_4^2 via aqueous-phase S(IV) oxidation by H_2O_2, PACD, and MEPX. The increase in SO_4^{2-} production via the gas-phase SO_2 oxidation by HO and the aqueous-phase S(IV) oxidation by O_3 overwhelms the reduction in SO_4^{2-} production via aqueous-phase S(IV) oxidation by H_2O_2, PACD, and MEPX, resulting in the net increase in SO_4^{2-} predictions with RACM2. Increased SO_4^{2-} also translates to enhanced particulate ammonium NH_4^+. Higher HNO_3 also leads to more partitioning to particulate nitrate NO_3^- compared to the CB05TU simulation.

Ambient monitoring data from the CASTNET network are used to compare model predictions for SO_4^{2-}, NO_3^-, and NH_4^+ (Fig. 10c–e). While CB05TU captures

SO_4^{2-} measurements at the lower observed levels, it substantially under-predicts at higher observed concentrations. However, RACM2 improves the comparisons with observed data by reducing the under-predictions at the higher observed concentrations. The slope of the fitted line of CB05TU predictions and observed data is 0.85 while the value for RACM2 is 0.95. Measured NO_3^- from the CASTNET sites are compared to model predictions in Fig. 10d. RACM2 predictions generally are similar to or better than the CB05TU predictions. Measured NH_4^+ from the CASTNET sites are compared to model predictions in Fig. 10e. CB05TU under-predicts the observed data especially at the higher observed concentrations. RACM2 improves the comparisons with observed data by lowering the underpredictions. Similar to the comparison with observed data from CASTNET, RACM2 also improves the comparison of predicted SO_4^{2-}, NO_3^-, and NH_4^+ to observations from the Interagency Monitoring of PROtected Visual Environments (IMPROVE) network and the Speciation Trends Network (STN). The impacts of RACM2 on inorganic aerosols in the US are similar to those reported by Kim et al. (2011) for Europe. RACM2 enhances the predicted domain-wide mean $PM_{2.5}$ by 7 % (Table 3) compared to CB05TU. Kim et al. (2011) reported an enhancement of 6 % for $PM_{2.5}$ over the Europe.

3.5.2 Impact on secondary organic aerosols

CB05TU predicted monthly mean SOA concentrations exceed 0.2 $\mu g\,m^{-3}$ in most of the modeling domain (Fig. 11a). The largest concentrations are predicted in the Southeastern US, Northwestern US, and California. RACM2 increases SOA across the entire US compared to CB05TU. It increases SOA by 12–20 % over a large portion of the eastern and western US and by 4–12 % in other areas (Fig. 11b). Higher predicted oxidant levels (OH and O_3) in RACM2 result in higher production of semivolatile organic compounds from oxidation of volatile organic compounds and consequently higher SOA from both biogenic and anthropogenic precursors. It also increases the in-cloud SOA though the overall contribution of in-cloud SOA to total SOA is generally small. Impacts

of RACM2 on SOA are different than those reported by Kim et al. (2011) over Europe due to the differences in the SOA chemistry between the two models. Predicted monthly mean Secondary Organic Carbon (OC_{sec}) obtained with the two mechanisms are compared to estimates inferred from observed data at IMPROVE sites (Fig. 11c). Mean observed OC_{sec} concentrations are derived using the procedures described by Yu et al. (2004) which uses $(OC/EC)_{pri}$ ratio, observed EC and OC to calculate OC_{sec}. The model with CB05TU under-predicts observed data by 0.25 $\mu g\,m^{-3}$ while the model with RACM2 under-predicts observed OC_{sec} by 0.19 $\mu g\,m^{-3}$. Thus, RACM2 improves the model comparison with observed SOA.

4 Impact on air pollution control strategy

Air pollution control strategies are developed by performing model simulations with normal and reduced emissions and determining relative responses of the model. A Relative Reduction Factor (RRF) is a commonly used parameter which is estimated by dividing the predicted concentrations with reduced emissions to those obtained with normal emissions (Jones et al., 2005).

4.1 Impact on O_3 control strategy

Two additional model simulations were performed for a 10-day period in September with a 25 % NO_x emission reduction with each mechanism. RRFs are estimated for each mechanism by dividing the predicted average O_3 obtained with reduced emissions to those obtained with normal emissions. Estimated RRFs with CB05TU are presented in Fig. 12a. An RRF of less than 1.0 suggests that predicted O_3 decreases with reduced NO_x emissions while an RRF of more than 1.0 suggests that predicted O_3 increases with reduced NO_x emissions. Predictions of O_3 generally increase with reduced NO_x emissions in urban areas. Differences in the RRFs between RACM2 and CB05TU are presented in Fig. 12b. Small negative values are found in northwest US

and isolated areas in the Midwest while small positive values are found in the southern US. Both mechanisms exhibit similar representativeness in O_3 to perturbations in NO_x emissions. Thus, any control strategies developed using the two mechanisms for improving O_3 are not expected to be substantially different.

4.2 Impact on $PM_{2.5}$ control strategy

Two other model simulations were performed for the 10-day period with a 25 % SO_2 emissions reduction: one with CB05TU and the other with RACM2. RRFs were estimated for each mechanism by dividing the predicted average $PM_{2.5}$ obtained with reduced emissions to those obtained with normal emissions. Estimated RRFs with CB05TU are presented in Fig. 13a. RRF values are close to 1.0 for many areas which suggest that $PM_{2.5}$ does not decrease in these areas with a 25 % SO_2 emissions reduction. The lowest RRF values over the land are found in the southeastern US and Mexico which suggests this region benefits more from the SO_2 reduction than other areas. The SO_2 emissions reduction also shows appreciable benefit in the Midwest and surrounding areas. Differences in the RRFs between RACM2 and CB05TU are presented in Fig. 13b. Small negative values are obtained for many areas which suggest the use of RACM2 produces marginally greater $PM_{2.5}$ reduction with a 25 % SO_2 emissions control. Thus, the impacts of the two mechanisms on RRFs for SO_2 emissions perturbation are also small.

Similar RRFs for $PM_{2.5}$ were estimated for each mechanism for simulations involving 25 % reduction in NO_x emissions (Fig. 13c). The lowest RRFs are found in the Midwest and surrounding areas which suggests this region benefits more from the NO_x control than other areas. RRF values are close to 1.0 for many areas which suggest $PM_{2.5}$ does not decrease in these areas with 25 % NO_x emissions reduction. Differences in the RRFs between RACM2 and CB05TU are presented in Fig. 13d. Small negative values are found in the Midwest and other areas while positive values are found in isolated areas. Thus, the impacts of the two mechanisms on RRFs for NO_x emissions

control are small. Thus, both mechanisms exhibit similar RRFs for $PM_{2.5}$ in response to SO_2 and NO_x emissions perturbations.

5 Summary and conclusions

We have implemented RACM2 into the CMAQ modeling system and performed month long simulations to benchmark its impacts on model predictions relative to the CB05TU mechanism as well as observed data. Model predictions of many chemical species obtained with the two mechanisms differ by relatively large margins. Predicted HO, TNO_3, and OPE obtained with RACM2 are greater than those obtained with CB05TU while predicted H_2O_2, MEPX, PACD, PAN, NTR, and NO_z concentrations obtained with RACM2 are lower than those obtained with CB05TU. A comparison of model predictions with the available observed data suggests that predictions obtained with RACM2 for most species agree better with the observed data. Predicted O_3 concentrations obtained with RACM2 are greater than those obtained with CB05TU. At low observed O_3 levels, CB05TU tends to over-predict O_3 and RACM2 further over-predicts in such conditions. However, CB05TU under-predicts O_3 when observed values are greater than 70 ppbv while RACM2 improves the predictions for such conditions. OPE inferred from RACM2 agree better with the observed data than those from CB05TU. Predicted secondary inorganic and organic aerosols obtained with RACM2 are greater compared to those obtained with CB05TU which leads to improved agreements with the observed data. While the two mechanisms produce relatively large differences in the predictions of O_3 and secondary particles, any air pollution control strategies developed for improving O_3 and $PM_{2.5}$ are not expected to be noticeably different.

Disclaimer

Although this paper has been reviewed by EPA and approved for publication, it does not necessarily reflect EPA's policies or views.

Acknowledgements. The authors would like to thank Ryan Cleary of Computer Sciences Corporation for preparing model-ready emissions and Enhwa (Nancy) Hwang for performing CMAQ model simulations used in this study.

References

Appel, K. W., Gilliland, A. B., Sarwar, G., and Gilliam, R. C.: Evaluation of the Community Multiscale Air Quality (CMAQ) model version 4.5: sensitivities impacting model performance, Part I – Ozone, Atmos. Environ., 41, 9603–9615, 2007.

Appel, K. W., Pouliot, G., Simon, H., Sarwar, G., Pye, H. O. T., Napelenok, S., Akhtar, F., Roselle, S. J.: Evaluation of dust and trace metal estimates from the Community Multiscale Air Quality (CMAQ) model version 5.0, Geosci. Model Dev. Discuss., 6, 1859–1899, doi:10.5194/gmdd-6-1859-2013, 2013.

Arnold, J. R. and Dennis, R. L.: Testing CMAQ chemistry sensitivities in base case and emissions control runs at SEARCH and SOS99 surface sites in the southeastern US, Atmos. Environ., 40, 5027–5040, 2006.

Arnold, J. R., Dennis, R. L., and Tonnesen, G. S.: Diagnostic evaluation of numerical air quality models with specialized ambient observations: testing the Community Multiscale Air Quality Modeling System (CMAQ) at selected SOS 95 ground sites, Atmos. Environ., 37, 1185–1198, 2003.

Atkinson, R., Baulch, D. L., Cox, R. A., Crowley, J. N., Hampson, R. F., Hynes, R. G., Jenkin, M. E., Kerr, J. A., Rossi, M. J., and Troe, J.: Summary of evaluated kinetic and photochemical data for atmospheric chemistry – IUPAC subcommittee on gas kinetic data evaluation for atmospheric chemistry, available at: http://www.iupac-kinetic.ch.cam.ac.uk/index.html, last access: 8 December 2005, 2005.

Bey, I., Jacob, D. J., Yantosca, R. M., Logan, J. A., Field, B. D., Fiore, A. M., Li, Q., Liu, H. Y., Mickley, L. J., and Schultz, M. G.: Global modeling of tropospheric chemistry with assimilated meteorology: model description and evaluation, J. Geophys. Res., 106, 23073–23096, 2001.

Binkowski, F. S. and Roselle, S. J.: Community Multiscale Air Quality (CMAQ) model aerosol component, I: model description, J. Geophys. Res., 108, 4183, doi:10.1029/2001JD001409, 2003.

Byun, D. and Schere, K. L.: Review of the governing equations, computational algorithms, and other components of the Models-3 Community Multiscale Air Quality (CMAQ) modeling system, Appl. Mech. Rev., 59, 51–77, 2006.

Cai, C., Kelly, J. T., Avise, J. C., Kaduwela, A. P., and Stockwell, W. R.: Photochemical modeling in California with two chemical mechanisms: model intercomparison and response to emissions reductions, J. Air Waste Manage., 61, 559–572, 2011.

Carlton, A. G., Turpin, B. J., Altieri, K. E., Seitzinger, S. P., Mathur, R., Roselle, S. J., and Weber, R. J.: CMAQ model performance enhanced when in-cloud SOA is included: comparisons of OC predictions with measurements, Environ. Sci. Technol., 42, 8798–8802, 2008.

Carlton, A. G., Bhave, P. V., Napelenok, S. L., Edney, E. O., Sarwar, G., Pinder, R. W., Pouliot, G. A., and Houyoux, M.: Model representation of secondary organic aerosol in CMAQv4.7, Environ. Sci. Technol., 44, 8553–8560, 2010.

Carter, W. P. L.: A detailed mechanism for the gas-phase atmospheric reactions of organic compounds, Atmos. Environ., 24, 481–518, 1990.

Carter, W. P. L.: Documentation of the SAPRC-99 Chemical Mechanism for VOC Reactivity Assessment, Report to the California Air Resources Board, available at: http://www.engr.ucr.edu/~carter/reactdat.htm, last access: 8 March 2013, 2000.

Carter, W. P. L.: Development of the SAPRC-07 chemical mechanism, Atmos. Environ., 44, 5324–5335, 2010.

Davis, J. M., Bhave, P. V., and Foley, K. M.: Parameterization of N_2O_5 reaction probabilities on the surface of particles containing ammonium, sulfate, and nitrate, Atmos. Chem. Phys., 8, 5295–5311, doi:10.5194/acp-8-5295-2008, 2008.

Eder, B. and Yu, S.: A performance evaluation of the 2004 release of Models-3 CMAQ, Atmos. Environ., 40, 4811–4824, 2006.

Faraji, M., Kimura, Y., McDonald-Buller, E., and Allen, D.: Comparison of the Carbon Bond and SAPRC photochemical mechanisms under conditions relevant to southeast Texas, Atmos. Environ., 42, 5821–5836, 2008.

Foley, K. M., Roselle, S. J., Appel, K. W., Bhave, P. V., Pleim, J. E., Otte, T. L., Mathur, R., Sarwar, G., Young, J. O., Gilliam, R. C., Nolte, C. G., Kelly, J. T., Gilliland, A. B., and Bash, J. O.: Incremental testing of the Community Multiscale Air Quality (CMAQ) modeling system version 4.7, Geosci. Model Dev., 3, 205–226, doi:10.5194/gmd-3-205-2010, 2010.

Fountoukis, C. and Nenes, A.: ISORROPIA II: a computationally efficient thermodynamic equilibrium model for K^+–Ca^{2+}–Mg^{2+}–NH_4^+–Na^+–SO_4^{2-}–NO_3^-–Cl^-–H_2O aerosols, Atmos. Chem. Phys., 7, 4639–4659, doi:10.5194/acp-7-4639-2007, 2007.

Gery, M. W., Whitten, G. Z., Killus, J. P., and Dodge, M. C.: A photochemical kinetics mechanism for urban and regional scale computer modeling, J. Geophys. Res., 94, 12925–12956, 1989.

Gilliam, R. C. and Pleim, J. E.: Performance assessment of new land-surface and planetary boundary layer physics in the WRF-ARW, J. Appl. Meteorol. Clim., 49, 760–774, 2010.

Gilliam, R. C., Godowitch, J. M., and Rao, S. T.: Improving the horizontal transport in the lower troposphere with four dimensional data assimilation, Atmos. Environ., 53, 186–201, 2012.

Goliff, W. S., Stockwell, W. R., and Lawson, C. V.: The regional atmospheric chemistry mechanism, version 2, Atmos. Environ., 68, 174–185, 2013.

Houyoux, M. R., Vukovich, J. M., Coats Jr., C. J., Wheeler, N. M., and Kasibhatla, P. S.: Emission inventory development and processing for the seasonal model for regional air quality (SMRAQ) project, J. Geophys. Res., 105, 9079–9090, 2000.

Hutzell, W. T., Luecken, D. J., Appel K. W., and Carter, W. P. L.: Interpreting predictions from the SAPRC07 mechanism based on regional and continental simulations, Atmos. Environ., 46, 417–429, 2012.

IUPAC: IUPAC subcommittee for gas kinetic data evaluation, http://www.iupac-kinetic.ch.cam.ac.uk/, 2010.

Jones, J. M., Hogrefe, C., Henry, R. F., Ku, J. Y., and Sistla, G.: An assessment of the sensitivity and reliability of the relative reduction factor approach in the development of 8-hr ozone attainment plans, J. Air Waste Manage., 55, 13–19, 2005.

Kim, Y., Sartelet, K., and Seigneur, C.: Comparison of two gas-phase chemical kinetic mechanisms of ozone formation over Europe, J. Atmos. Chem., 62, 89–119, 2009.

Kim, Y., Sartelet, K., and Seigneur, C.: Formation of secondary aerosols over Europe: comparison of two gas-phase chemical mechanisms, Atmos. Chem. Phys., 11, 583–598, doi:10.5194/acp-11-583-2011, 2011.

Kleinman, L. I., Daum, P. H. Lee, Y.-N., Nunnermacker, L. J., Springston, S. R., Weinstein-Lloyd, J., and Rudolph, J.: Ozone production efficiency in an urban area, J. Geophys. Res., 107, 4733, doi:10.1029/2002JD002529, 2002.

Luecken, D. J., Phillips, S., Sarwar, G., and Jang, C.: Effects of using the CB05 vs. SAPRC99 vs. CB4 chemical mechanism on model predictions: ozone and gas-phase photochemical precursor concentrations, Atmos. Environ., 42, 5805–5820, 2008.

Mao, J., Ren, X., Chen., S., Brune, W. H., Chen, Z., Martinez, M., Harder, H., Lefer, B., Rappenglück, B., Flynn, J., and Leuchner, M.: Atmospheric oxidation capacity in the summer of Houston 2006: comparison with summer measurements in other metropolitan studies, Atmos. Environ., 44, 4107–4115, 2010a.

Mao, H., Chen, M., Hegarty, J. D., Talbot, R. W., Koermer, J. P., Thompson, A. M., and Avery, M. A.: A comprehensive evaluation of seasonal simulations of ozone in the northeastern US during summers of 2001–2005, Atmos. Chem. Phys., 10, 9–27, doi:10.5194/acp-10-9-2010, 2010b.

Mollner, A. K., Valluvadasan, S., Feng, L., Sprague, M. K., Okumura, M., Milligan, D. B., Bloss, W. J., Sander, S. P., Martien, P. T., Harley, R. A., McCoy, A. B., and Carter, W. P. L.: Rate of gas phase association of hydroxyl radical and nitrogen dioxide, Science, 330, 646–649, 2010.

Parrish, D. D., Allen, D. T., Bates, T. S., Estes, M., Fehsenfeld, F.C., Feingold, G., Ferrare, R., Hardesty, R. M., Meagher, J. F., Nielsen-Gammon, J. W., Pierce, R. B., Ryerson, T. B., Seinfeld, J. H., and Williams, E. J.: Overview of the second Texas Air Quality Study (TexAQS II) and the Gulf of Mexico Atmospheric Composition and Climate Study (GoMACCS), J. Geophys. Res., 114, D00F13, doi:10.1029/2009JD011842, 2009.

Pouliot, G., Pierce, T., Gon, H. D. V. D., Schaap, M., Moran, M., and Nopmongcol, U.: Comparing emission inventories and model-ready emission datasets between Europe and North America for the AQMEII project, Atmos. Environ., 53, 4–14, 2012.

Sander, S. P., Friedl, R. R., Ravishankara, A. R., Golden, D. M., Kolb, C. E., Kurylo, M. J., Huie, R. E., Orkin, V. L., Molina, M. J., Morrtgat, G. K., Finlayson-Pitts, B. J.: Chemical kinetics and photochemical data for use in atmospheric studies, evaluation number 14, NASA Jet Propulsion Laboratory, available at: http://jpldataeval.jpl.nasa.gov/download.html (last access: 8 March 2013), 2003.

Sander, S. P., Abbatt, J. P. D., Barker, J. R., Burkholder, J. B., Friedl, R. R., Golden, D. M., Huie, R. E., Kolb, C. E., Kurylo, M. J., Moortgat, G. K., Orkin, V. L., and Wine, P. H.: Chemical Kinetics and Photochemical Data for Use in Atmospheric Studies, Evaluation No. 17, Jet Propulsion Laboratory, Pasadena, CA, 2011.

Sandu, A., Verwer, J. G., Blom, J. G., Spee, E. J., Carmichael, G. R., and Potra, F. A.: Benchmarking stiff ODE solvers for atmospheric chemistry problems II: Rosenbrock solvers, Atmos. Environ., 31, 3459–3472, 1997.

Sarwar, G., Roselle, S., Mathur, R., Appel, W., and Philbrick, C. R.: A comparison of Community Multiscale Air Quality (CMAQ) modeling system predictions with observations from the Northeast Oxidant and Particle Study, Abstract # 342, in: 100th Annual Conference & Exhibition of the Air & Waste Management Association, 26–28 June 2007, Pittsburgh, PA, 2007.

Sarwar, G., Luecken, D., Yarwood, G., Whitten, G., and Carter, B.: Impact of an updated Carbon Bond mechanism on air quality using the Community Multiscale Air Quality modeling system: preliminary assessment, J. Appl. Meteorol. Clim., 47, 3–14, 2008.

Sarwar, G., Appel, K. W., Carlton, A. G., Mathur, R., Schere, K., Zhang, R., and Majeed, M. A.: Impact of a new condensed toluene mechanism on air quality model predictions in the US, Geosci. Model Dev., 4, 183–193, doi:10.5194/gmd-4-183-2011, 2011.

Sarwar, G., Fahey, F., Kwok, R., Gilliam, R., Xue, J., Jianzhen, Y., and Carter, W. P. L.: Examining the potential impacts of the aqueous-phase S(IV) oxidation by NO_2 and the gas-phase SO_2 oxidation by the Stabilized Criegee Intermediate on sulfate, Atmos. Environ., 68, 186–197, 2013.

Schwede, D., Pouliot, G., and Pierce, T.: Changes to the biogenic emissions inventory system version 3 (BEIS3), in: 4th Annual CMAS Models-3 Users' Conference, 26–28 September 2005, UNC-Chapel Hill, NC, 1–6, available at: http://www.cmascenter.org/conference/2005/abstracts/2_7.pdf (last access: 8 March 2013), 2005.

Seigneur, C. and Saxena, P.: A theoretical investigation of sulfate formation in clouds, Atmos. Environ., 22, 101–115, 1988.

Shearer, M. S., Harley, R. A., Jin, L., and Brown, N. J.: Comparison of SAPRC99 and SAPRC07 mechanisms in photochemical modeling for central California, Atmos. Environ., 46, 205–216, 2012.

Skamarock, W. C., Klemp, J. B., Dudhia, J., Grill, D. O., Barker, D. M., Duda, M. G, Huang, X.-Y., Wang, W., and Powers, J. G.: A description of the advanced research WRF version 3. NCAR Tech Note NCAR/TN 475 STR, UCAR Communications, P.O. Box 3000, Boulder, CO 80307, 125 pp., 2008.

Stockwell, W. R.: A homogeneous gas phase mechanism for use in a regional acid deposition model, Atmos. Environ., 20, 1615–1632, 1986.

Stockwell W. R., Middleton, P., Chang, J. S., and Tang, X.: The second generation Regional Acid Deposition Model chemical mechanism for regional air quality modeling, J. Geophys. Res., 95, 16343–16367, 1990.

Stockwell, W. R., Kirchner, F., Kuhn, M., and Seefeld, S.: A new mechanism for regional atmospheric chemistry modeling, J. Geophys. Res., 102, 25847–25879, 1997.

Trainer, M., Parish, D. D., Goldan, P. D., Roberts, J., and Fehsenfeld, F. C.: Review of observation-based analysis of the regional factors influencing ozone concentrations, Atmos. Environ., 34, 2045–2061, 2000.

Yarwood, G., Rao, S., Yocke, M., and Whitten, G.: Updates to the Carbon Bond Chemical Mechanism: CB05, Final Report to the US EPA, RT-0400675, available at: http://www.camx.com (last access.: 8 March 2013), 2005.

Yu, S., Dennis, R. L., Bhave, P. V., and Eder, B. K.: Primary and secondary organic aerosols over the United States: estimates on the basis of observed organic carbon (OC) and elemental carbon (EC), and air quality modeled primary OC/EC ratios, Atmos. Environ., 38, 5257–5268, 2004.

Yu, S., Mathur, R., Sarwar, G., Kang, D., Tong, D., Pouliot, G., and Pleim, J.: Eta-CMAQ air quality forecasts for O_3 and related species using three different photochemical mechanisms (CB4, CB05, SAPRC-99): comparisons with measurements during the 2004 ICARTT study, Atmos. Chem. Phys., 10, 3001–3025, doi:10.5194/acp-10-3001-2010, 2010.

Yu, S., Mathur, R., Pleim, J., Pouliot G., Wand, D., Eder, B., Schere, K., Gilliam, R., and Rao, S. T.,: Comparative evaluation of the impact of WR–NMM and WR–ARW meteorology on CMAQ simulations for O_3 and related species during the 2006 TexAQS/GoMACCS campaign, Atmos. Poll. Res., 3, 149–162, 2012.

Whitten, G. Z., Heo., G., Kimura, Y., McDonald-Buller, E., Allen, D., Carter, W. P. L., and Yarwood, G.: A new condensed toluene mechanism for Carbon Bond: CB05-TU, Atmos. Environ., 44, 5346–5355, 2010.

Zhang, X., Chen, Z. M., He, S. Z., Hua, W., Zhao, Y., and Li, J. L.: Peroxyacetic acid in urban and rural atmosphere: concentration, feedback on PAN-NO_x cycle and implication on radical chemistry, Atmos. Chem. Phys., 10, 737–748, doi:10.5194/acp-10-737-2010, 2010.

Table 1. Model chemical species in CB05TU* (Yarwood et al., 2005; Whitten et al., 2010).

Species Name	Description	Species Name	Description
NO	Nitric oxide	MEO2	Methylperoxy radical
NO2	Nitrogen dioxide	MEOH	Methanol
O3	Ozone	MEPX	Methylhydroperoxide
O	Oxygen atom (triplet)	FACD	Formic acid
O1D	Oxygen atom (singlet)	ETHA	Ethane
OH	Hydroxyl radical	ROOH	Higher organic peroxide
HO2	Hydroperoxy radical	AACD	Higher carboxylic acid
H2O2	Hydrogen peroxide	PACD	Higher peroxycarboxylic acid
NO3	Nitrate radical	PAR	Paraffin carbon bond
N2O5	Dinitrogen pentoxide	ROR	Secondary alkoxy radical
HONO	Nitrous acid	ETH	Ethene
HNO3	Nitric acid	OLE	Terminal olefin carbon bond
PNA	Peroxynitric acid	IOLE	Internal olefin carbon bond
CO	Carbon monoxide	ISOP	Isoprene
FORM	Formaldehyde	ISPD	Isoprene product
ALD2	Acetaldehyde	TERP	Terpene
C2O3	Acetylperoxy radical	TOL	Toluene & other monoalkyl aromatics
PAN	Peroxyacetyl nitrate	XYL	Xylene and other polyalkyl aromatics
ALDX	Higher aldehyde	CRES	Cresol and higher MW weight phenols
CXO3	Higher acylperoxy radical	TO2	Toluene-hydroxyl radical adduct
PANX	Higher peroxyacyl nitrate	OPEN	Aromatic ring opening product
XO2	NO to NO_2 conversion (from RO_2)	CRO	Methylphenoxy radical
XO2N	NO to RNO_3 conversion (from RO_2)	MGLY	Methylglyoxal and related products
NTR	Organic nitrate (RNO_3)	SO2	Sulfur dioxide
ETOH	Ethanol	SULF	Sulfuric acid (gaseous)
CAT1	Methyl-catechol	HCO3	Adduct formed from FORM and HO_2
CRON	Nitro-cresol	CRN2	Peroxy radical from nitro-cresol
CRNO	Alkoxy radical from nitro-cresol	CRPX	Nitro-cresol from hydroperoxide
CAO2	Peroxy radical from CAT1	OPAN	PAN from OPO_3
OPO3	Peroxy radical from OPEN		

* N_2 (nitrogen), H_2 (hydrogen), H_2O (water vapor), M (air), O_2 (oxygen), CH_4 (methane) are not listed. Prescribed constant concentrations are used in CMAQ for these species except H_2O which are used from meteorological files.

Table 2. Model chemical species in RACM2* (Goliff et al., 2012).

Species Name	Description	Species Name	Description
CO	Carbon monoxide	ISOP	Peroxy radicals formed from ISO + HO
NO	Nitric oxide	KET	Ketones
NO2	Nitrogen dioxide	KETP	Peroxy radicals formed from KET
O3	Ozone	LIM	d-limonene and other cyclic diene-terpenes
O3P	Ground state oxygen atom	LIMP	Peroxy radicals formed from LIM
O1D	Excited state oxygen atom	MACP	Peroxy radicals formed from MACR + HO
HO	Hydroxyl radical	MACR	Methacrolein
HO2	Hydroperoxy radical	MAHP	Hydroperoxides from MACP + HO_2
H2O2	Hydrogen peroxide	MCP	Methyl peroxy radical from MACR + HO which does not form MPAN
NO3	Nitrate radical	MCT	Methyl catechol
N2O5	Dinitrogen pentoxide	MCTO	Alkoxy radical formed from MCT + HO and MCT + NO_3
HONO	Nitrous acid	MCTP	Radical formed from MCT + O_3 reaction
HNO3	Nitric acid	MEK	Methyl ethyl ketone
HNO4	Peroxynitric acid	MEKP	Peroxy radicals formed from MEK
SO2	Sulfur dioxide	MGLY	Methylglyoxal and other alpha-carbonyl aldehydes
SULF	Sulfuric acid	MO2	Methyl peroxy radical
ACD	Acetaldehyde	MOH	Methanol
ACE	Acetylene	MPAN	Peroxymethacryloylnitrate and other higher peroxyacylnitrates from isoprene oxidation
ACO3	Acetyl peroxy radicals	MVK	Methyl vinyl ketone
ACT	Acetone	MVKP	Peroxy radicals formed from MVK
ACTP	Peroxy radicals formed from ACT	NALD	Nitrooxyacetaldehyde
ADCN	Aromatic-NO_3 adduct from PHEN	OLI	Internal alkenes
ADDC	Aromatic-HO adduct from CSL	OLIP	Peroxy radicals formed from OLI
ALD	C3 and higher aldehydes	OLND	NO_3-alkene adduct reacting via decomposition
API	Alpha-pinenes & other cyclic terpenes with one double bond	OLNN	NO_3-alkene adduct reacting to form carbonitrates + HO_2
APIP	Peroxy radicals formed from API	OLT	Terminal alkenes
BALD	Benzaldehyde and other aromatic aldehydes	OLTP	Peroxy radicals formed from OLT
BALP	Peroxy radicals formed from BALD	ONIT	Organic nitrate
BAL1	Peroxy radicals formed from BALD	OP1	Methyl hydrogen peroxide
BAL2	Peroxy radicals formed from BALD	OP2	Higher organic peroxides

* N_2 (nitrogen), H_2 (hydrogen), H_2O (water vapor), M (air), O_2 (oxygen), CH_4 (methane) are not listed. Prescribed constant concentrations are used in CMAQ for these species except H_2O which are used from meteorological files. CO_2 used in the original mechanism is not used in CMAQ.

Table 2. Continued.

Species Name	Description	Species Name	Description
BEN	Benzene	ORA1	Formic acid
BENP	Peroxy radicals formed from BEN	ORA2	Acetic acid and higher acids
CHO	Phenoxy radical formed from CSL	ORAP	Peroxy radical formed from ORA2 + HO reaction
CSL	Cresol and other hydroxy substituted aromatics	PAA	Peroxyacetic acids and higher analogs
DCB1	Unsaturated dicarbonyls	PAN	Peroxyacetyl nitrate and higher saturated PANs
DCB2	Unsaturated dicarbonyls	PER1	Peroxy intermediate formed from TOL
DCB3	Unsaturated dicarbonyls	PER2	Peroxy intermediate formed from TOL
DIEN	Butadiene and other anthropogenic dienes	PHEN	Phenol
EOH	Ethanol	PHO	Phenoxy radical formed from phenol
EPX	Epoxide formed in TOL, XYL and XYO reactions	PPN	Peroxypropionyl nitrate
ETE	Ethene	RCO3	Higher saturated acyl peroxy radicals
ETEG	Ethylene glycol	ROH	C3 and higher alcohols
ETEP	Peroxy radicals formed from ETE	TLP1	Peroxy radicals formed from TOL
ETH	Ethane	TOL	Toluene and less reactive aromatics
ETHP	Peroxy radicals formed from ETH	TOLP	Peroxy radicals formed from TOL
GLY	Glyoxal	TR2	Peroxy radicals formed from TOL
HC3	Alkanes, alcohols, esters and alkynes with HO rate constant (298 K, 1 atm) less than 3.4×10^{-12} $cm^3 s^{-1}$	UALD	Unsaturated aldehydes
HC3P	Peroxy radicals formed from HC_3	UALP	Peroxy radicals formed from UALD
HC5	Alkanes, alcohols, esters and alkynes with HO rate constant (298 K, 1 atm) between 3.4×10^{-12} and 6.8×10^{-12} $cm^3 s^{-1}$	XO2	Accounts for addition NO to NO_2 conversions
HC5P	Peroxy radicals formed from HC_5	XY2	Peroxy radicals formed from XYL
HC8	Alkanes, alcohols, esters and alkynes with HO rate constant (298 K, 1 atm) greater than 6.8×10^{-12} $cm^3 s^{-1}$	XYO	o-xylene
HC8P	Peroxy radicals formed from HC_8	XYM	m-xylene
HCHO	Formaldehyde	XYP	p-xylene
HKET	Hydroxy ketone	XYL1	Peroxy radicals formed from XYL
ISHP	Beta-hydroxy hydroperoxides from ISOP + HO_2	XYLP	Peroxy radicals formed from XYL
ISO	Isoprene	XYO2	Peroxy radicals formed from XYO
ISON	Beta-hydroxyalkylnitrates from ISOP + NO alkylnitrates from ISO + NO_3	XYOP	Peroxy radicals formed from XYO

* N_2 (nitrogen), H_2 (hydrogen), H_2O (water vapor), M (air), O_2 (oxygen), CH_4 (methane) are not listed. Prescribed constant concentrations are used in CMAQ for these species except H_2O which are used from meteorological files. CO_2 used in the original mechanism is not used in CMAQ.

Table 3. A summary of the comparison of CB05TU and RACM2 predicted domain-wide monthly mean values.

Species	Unit	CB05TU	RACM2	Percent difference 100 × (RACM2 – CB05TU)/CB05TU
Hydroxyl radical (OH)	pptv	0.05	0.07	+46
Hydrogen peroxide (H_2O_2)	pptv	837	822	−2
Peroxyacetic acid (PACD)	pptv	400	26	−94
Methylhydroperoxide (MEPX)	pptv	492	398	−19
Total nitrate (TNO_3)	pptv	441	538	+22
Nitric acid (HNO_3)	pptv	289	364	+26
Peroxyacetyl nitrate (PAN)	pptv	232	141	−40
Organic nitrate (NTR)	pptv	378	222	−41
Secondary nitrogen (NO_z)	pptv	1305	1067	−18
Ozone (O_3)	ppbv	36.6	38.8	+6
Sulfate (SO_4^{2-})	$\mu g\,m^{-3}$	1.47	1.61	+10
Nitrate (NO_3^-)	$\mu g\,m^{-3}$	0.15	0.16	+6
Ammonium (NH_4^+)	$\mu g\,m^{-3}$	0.37	0.41	+10
Anthropogenic SOA	$\mu g\,m^{-3}$	0.07	0.10	+42
Biogenic SOA	$\mu g\,m^{-3}$	0.40	0.42	+5
In-cloud SOA	$\mu g\,m^{-3}$	0.01	0.011	+11
Fine particles ($PM_{2.5}$)	$\mu g\,m^{-3}$	4.6	4.9	+7

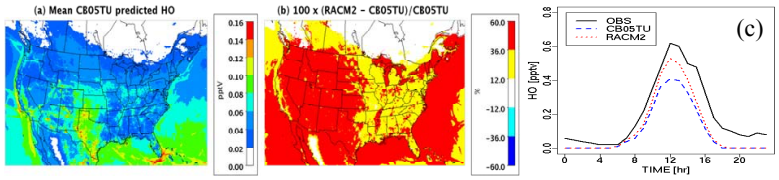

Fig. 1. (a) Predicted mean HO obtained with CB05TU **(b)** percent differences in mean HO between RACM2 and CB05TU **(c)** a comparison of predicted median HO to observed median data from the 2006 Texas Air Quality Study.

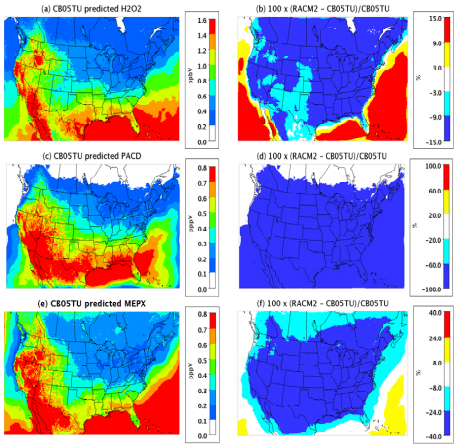

Fig. 2. (a) Predicted mean H_2O_2 obtained with CB05TU **(b)** percent differences in mean H_2O_2 between RACM2 and CB05TU **(c)** predicted mean PACD with CB05TU **(d)** percent differences in mean PACD between RACM2 and CB05TU **(e)** predicted mean MEPX obtained with CB05TU **(f)** percent differences in mean MEPX between RACM2 and CB05TU.

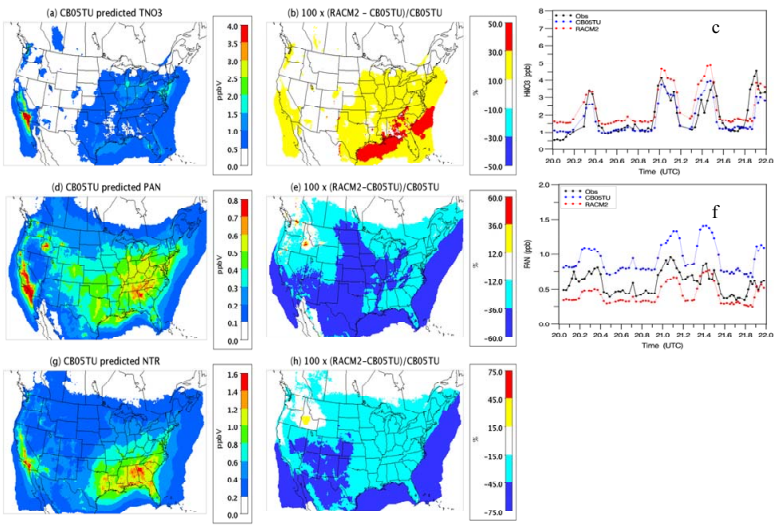

Fig. 3. (a) Predicted mean TNO_3 obtained with CB05TU **(b)** percent differences in mean TNO_3 between RACM2 and CB05TU **(c)** a comparison of predicted HNO_3 to measurements from the 2006 Texas Air Quality Study **(d)** predicted mean PAN obtained with CB05TU **(e)** percent differences in mean PAN between RACM2 and CB05TU **(f)** a comparison of predicted PAN to observed data from the 2006 Texas Air Quality Study **(g)** predicted mean NTR obtained with CB05TU **(h)** percent differences in mean NTR between RACM2 and CB05TU.

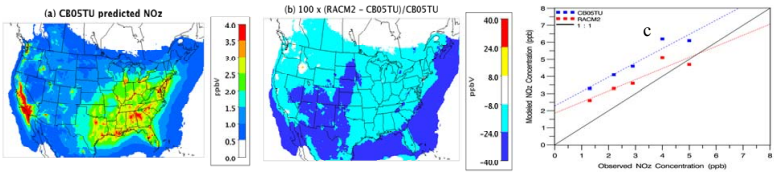

Fig. 4. (a) Predicted mean NO_z obtained with CB05TU **(b)** percent differences in mean NO_z between RACM2 and CB05TU **(c)** a comparison of predicted NO_z to measurements from the South Eastern Aerosol Research and Characterization.

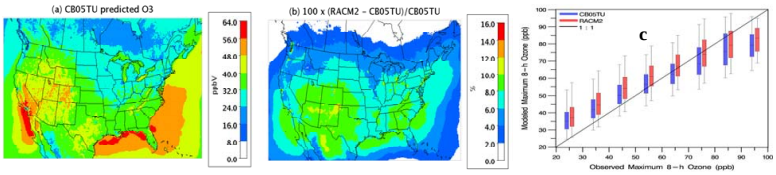

Fig. 5. (a) Predicted mean surface O_3 obtained with CB05TU **(b)** percent differences in mean O_3 between RACM2 and CB05TU **(c)** a comparison of predicted mean 8-h O_3 to observations from the Air Quality System.

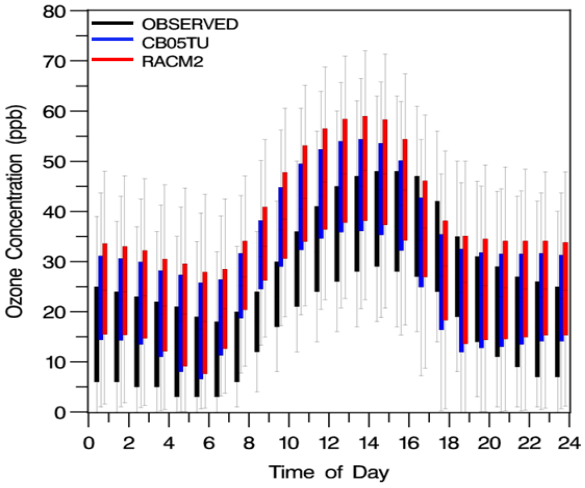

Fig. 6. A comparison of diurnal variation of predicted hourly surface O_3 obtained with CB05TU and RACM2 and observations from Air Quality System sites.

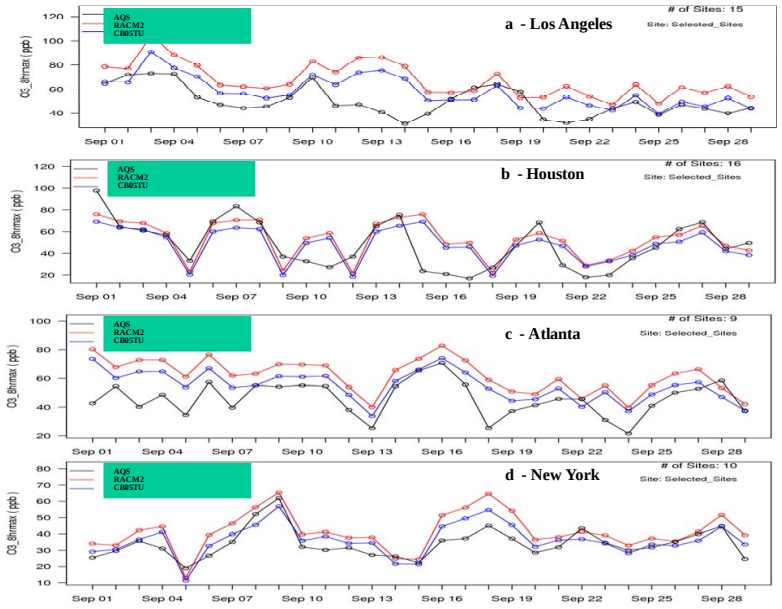

Fig. 7. Times series of predicted daily maximum 8-h O_3 with CB05TU and RACM2 and observations from **(a)** Los Angeles **(b)** Houston **(c)** Atlanta **(d)** New York.

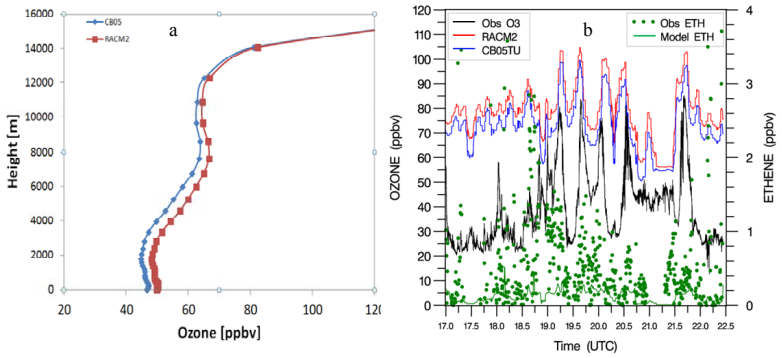

Fig. 8. (a) Predicted vertical O_3 profile obtained with CB05TU and RACM2 at 18:00 UTC on 13 September **(b)** a comparison of predicted aloft O_3 to aircraft measurements from the 2006 Texas Air Quality Study (15 September).

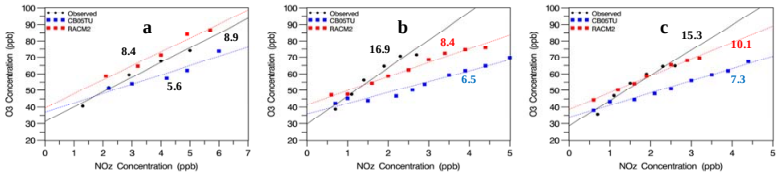

Fig. 9. A comparison of ozone production efficiency with values derived from observations from the Southeastern Aerosol Research and Characterization network sites **(a)** Yorkville, Georgia **(b)** Centreville, Alabama **(c)** Oak Grove, Mississippi.

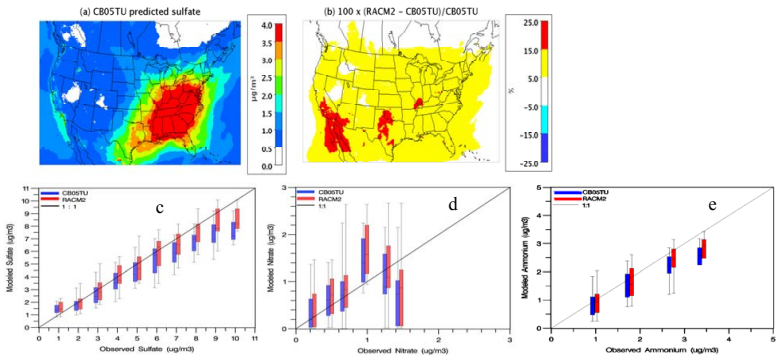

Fig. 10. (a) Predicted mean sulfate obtained with CB05TU **(b)** percent differences in mean sulfate between RACM2 and CB05TU **(c)** a comparison of predicted sulfate to measurements from the CASTNET sites **(d)** a comparison of predicted nitrate to measurements from the CASTNET sites **(e)** a comparison of predicted ammonium to measurements from the CASTNET sites.

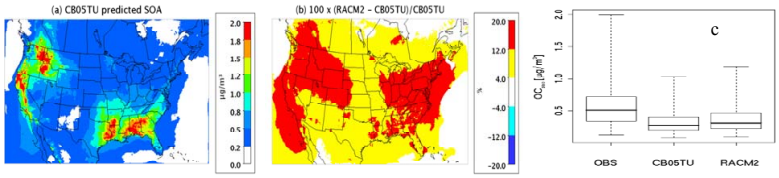

Fig. 11. (a) Predicted mean Secondary Organic Aerosols with CB05TU **(b)** percent differences in mean Secondary Organic Aerosols between RACM2 and CB05TU **(c)** a comparison of predicted mean Secondary Organic Carbon with values derived from the Interagency Monitoring of Protected Visual Environments network.

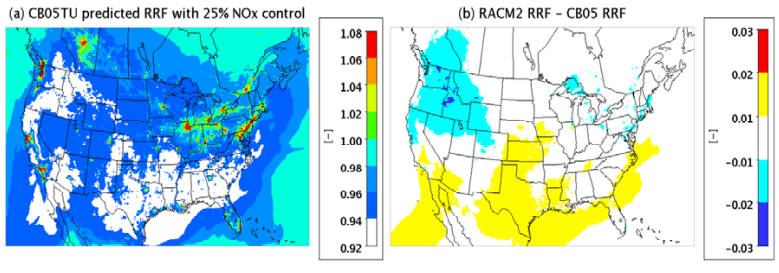

Fig. 12. (a) Relative Reduction Factors for ozone obtained with CB05TU due to 25 % NO_x control **(b)** differences in Relative Reduction for ozone between RACM2 and CB05TU due to 25 % NO_x control.

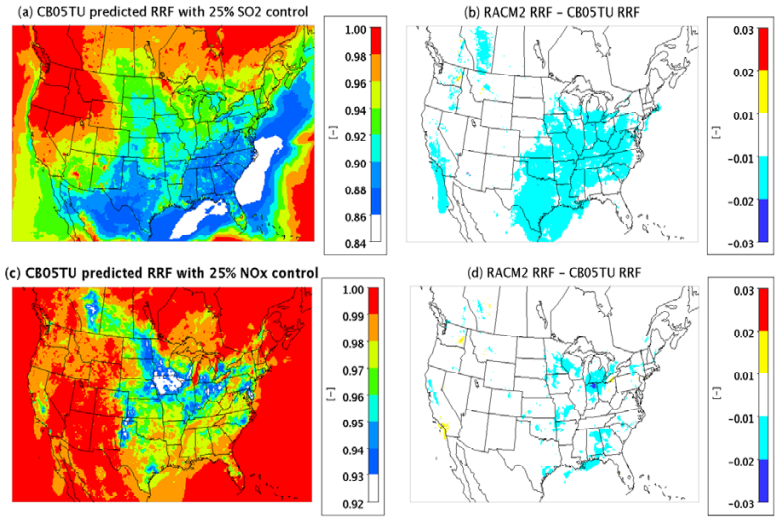

Fig. 13. (a) Relative Reduction Factors for $PM_{2.5}$ obtained with CB05TU due to 25 % SO_2 control **(b)** differences in Relative Reduction Factors for $PM_{2.5}$ between RACM2 and CB05TU due to 25 % SO_2 control **(c)** Relative Reduction Factors for $PM_{2.5}$ obtained with CB05TU due to 25 % NO_x control **(d)** differences in Relative Reduction Factors for $PM_{2.5}$ between RACM2 and CB05TU due to 25 % NO_x control.